RESEARCH PAPER

Formulation and Characterization of B-Cyclodextrin and Ethyl Cellulose-Based Nanosponges for Enhanced Solubility and Sustained Delivery of Prasugrel Hydrochloride

Suryawanshi A.N.[1], Ratnaparkhi M.P.[2]*

[1]*Research Scholar, Savitribai Phule Pune University, Pune 411041, Maharashtra, India*
[2]*Department of Pharmaceutics, Marathwada Mitra Mandal's College of Pharmacy, Thergaon, Pune 411033, Maharashtra, India*

Received:17th Aug, 2025; Revised: 5th Sep 2025; Accepted: 13th Nov, 2025; Available Online: 30th Nov, 2025

ABSTRACT
Prasugrel hydrochloride (Prasugrel HCl), a potent thienopyridine-class antiplatelet agent, is classified as a Biopharmaceutics Classification System (BCS) Class II drug, characterized by low aqueous solubility and high permeability, which limits its oral bioavailability. To address these challenges, nanosponges—three-dimensional, porous nanostructures—were developed using β-cyclodextrin (β-CD) and ethyl cellulose (EC) cross-linked with dichloromethane (DCM) via the emulsion solvent evaporation method. Four formulations (F1–F4) were prepared by varying polymer ratios and processing parameters. Preformulation studies confirmed PrasugrelHCl's physicochemical properties, including a melting point of 120.5–121.9°C, log P of 3.54, and poor water solubility (<0.1 mg/mL). Characterization revealed F3 (300 mg β-CD:200 mg EC, 1000 rpm stirring) as optimal, exhibiting 26.4% drug loading, 89.7% encapsulation efficiency, particle size of 268.4 nm, PDI of 0.278, and negative zeta potential (-27.2 mV) for stability. SEM analysis showed uniform spherical morphology with 60–120 nm pores in F3, while FTIR confirmed drug-excipient compatibility without chemical interactions. These nanosponges enhance solubility and enable sustained release, positioning F3 as a promising carrier for improved Prasugrel HCl delivery in cardiovascular therapy..
Keywords: Prasugrel HCl; Nanosponges; β-Cyclodextrin; Ethyl cellulose; Solubility enhancement; Antiplatelet therapy.
How to cite this article: Suryawanshi AN, Ratnaparkhi MP, Formulation and Characterization of β-Cyclodextrin and Ethyl Cellulose-Based Nanosponges for Enhanced Solubility and Sustained Delivery of Prasugrel Hydrochloride. Int J Drug Deliv Technol. 2025;15(4):1632-1640, DOI: 10.25258/ijddt.15.4.15
Source of support: Nil.
Conflict of interest: None

INTRODUCTION

Cardiovascular diseases remain a leading cause of morbidity and mortality worldwide, with acute coronary syndromes (ACS) often managed using dual antiplatelet therapy (DAPT) to prevent thrombotic events. Prasugrel hydrochloride (Prasugrel HCl), a third-generation thienopyridine $P2Y_{12}$ receptor antagonist, serves as a prodrug rapidly hydrolyzed in the intestine and activated via hepatic CYP3A4 and CYP2B6 to its active metabolite, R-138727, which irreversibly inhibits platelet aggregation for 7–10 days. Administered as 5–10 mg loading/maintenance doses in combination with aspirin, it demonstrates superior efficacy over clopidogrel in reducing ischemic events in percutaneous coronary intervention (PCI) patients, albeit with a slightly higher bleeding risk[1-3].

Despite its therapeutic promise, PrasugrelHCl's pharmacokinetics are hindered by its BCS Class II profile: aqueous solubility <0.1 mg/mL at pH 7 (practically insoluble), with pH-dependent dissolution (highly soluble at pH <2, sparingly soluble at pH 3–4). This low solubility contributes to variable bioavailability (approximately 80% in fasted state), influenced by gastric pH alterations from concomitant medications like proton pump inhibitors. Formulation strategies to enhance dissolution, such as nanosuspensions or cyclodextrin complexes, have shown promise, but sustained release remains elusive for optimizing DAPT compliance[4-6].

Nanosponges, hyper-cross-linked, colloidal nanoparticles (50–1000 nm) derived from cyclodextrins or polymers like ethyl cellulose, offer a versatile platform for encapsulating hydrophobic drugs within their porous nanocavities. Fabricated via emulsion solvent evaporation or diffusion, β-CD-based nanosponges leverage inclusion complexation for solubility augmentation (up to 100-fold) and controlled release via diffusion or erosion mechanisms. When combined with ethyl cellulose, a hydrophobic polymer, they form amphiphilic matrices ideal for BCS II drugs, improving entrapment efficiency (>80%) and mucoadhesion for gastrointestinal targeting[7-9].

This study aimed to develop and characterize β-CD/EC nanosponges for Prasugrel HCl, evaluating preformulation properties, formulation optimization, and in vitro attributes to establish F3 as a lead for enhanced bioavailability and reduced dosing frequency in antiplatelet therapy.

MATERIALS AND METHODS

Materials

**Author for Correspondence:*mukeshparkhi@yahoo.co.in

Prasugrel HCl (purity >99%) was obtained from Sigma-Aldrich (USA). β-Cyclodextrin (β-CD) and ethyl cellulose (EC, viscosity 45 cP) were sourced from HiMedia Laboratories (India). Dichloromethane (DCM, analytical grade) and polyvinyl alcohol (PVA, MW 30,000–70,000) were from Merck (India). All other solvents (methanol, ethanol, acetone, ethyl acetate, chloroform) and reagents (orthophosphoric acid) were of HPLC/analytical grade.

Preformulation Studies

Appearance: Visual inspection under white light. Melting Point: Determined using a digital capillary apparatus (Electothermal, UK) in triplicate (n=3). Solubility: Shake-flask method at 37±0.5°C for 24 h; qualitative classification per USP. Partition Coefficient (log P): Shake-flask method with octanol:water (1:1) at 37°C, equilibrated for 48 h, analyzed by UV at 254 nm. Calibration Curves: Prepared in distilled water (10–100 µg/mL, 218 nm) and methanol (5–200 µg/mL, 254 nm) using UV-Vis spectrophotometer (Shimadzu UV-1800, Japan). Linearity assessed by R^2. LOD/LOQ calculated per ICH Q2(R1). UV-Vis Spectra: Scanned 200–400 nm in methanol. HPLC Analysis: Reverse-phase on C18 column (250×4.6 mm, 5 µm); mobile phase acetonitrile:0.1% orthophosphoric acid (60:40 v/v, pH 3.0); flow 1.0 mL/min; detection 254 nm (Shimadzu LC-20AD). FTIR Spectra: KBr pellet method (4000–400 cm^{-1}) on FTIR spectrometer (PerkinElmer Spectrum Two, USA) [10-12].

Nanosponge Preparation

Nanosponges were prepared by emulsion solvent evaporation. EC (100–200 mg) was dissolved in 5 mL DCM. This organic phase was added dropwise to 50 mL aqueous PVA (0.5% w/v) containing β-CD (200–300 mg) under high-speed stirring (500–1000 rpm, Remi stirrer, India) for 2 h at 25°C. Solvent evaporated under reduced pressure (rotavapor, Heidolph, Germany) at 40°C for 4 h. Product washed with water, lyophilized (Labconco, USA), and stored at 4°C. Formulations: F1 (200 mg β-CD:100 mg EC, 500 rpm), F2 (250:150, 750 rpm), F3 (300:200, 1000 rpm), F4 (250:150, 1000 rpm + excess DCM) [13-15].

Characterization

Drug Loading and Encapsulation Efficiency: 10 mg nanosponge extracted in methanol, centrifuged (10,000 rpm, 10 min), supernatant analyzed by UV (254 nm). % Loading = (Drug loaded/Total nanosponge) × 100; EE% = (Actual loading/Theoretical loading) × 100 (n=3). Particle Size, PDI, Zeta Potential: Dynamic light scattering (Malvern Zetasizer Nano ZS, UK) in water (n=3). Surface Morphology: SEM (JEOL JSM-6390LV, Japan) at 15 kV, gold-sputtered samples. FTIR: As above, for pure drug, excipients, mixtures, and formulations[16-18].

Statistical analysis

Data analyzed using ANOVA (GraphPad Prism 8.0); $p<0.05$ significant[19].

RESULTS AND DISCUSSION

Preformulation

Preformulation investigations establish the foundational physicochemical properties of Prasugrel HCl, informing its compatibility with nanosponge excipients and predicting behavior in the delivery system. These studies ensure the drug's stability, solubility enhancement, and analytical method reliability.

Appearance

Prasugrel HCl, in its pure active pharmaceutical ingredient (API) form, presents as a white to off-white crystalline powder. This visual characteristic confirms the drug's purity and homogeneity, essential for reproducible formulation processing and quality control.

Melting Point

Using a digital melting point apparatus, Prasugrel HCl exhibited a sharp melting transition over the range of 120.5–121.9°C (**Table 1**). This moderate melting point reflects the drug's thermal stability and crystalline nature, which are advantageous for nanosponge encapsulation to prevent premature degradation during processing or storage. Deviations from this range in future formulations would signal potential impurities or polymorphic changes.

Table 1: Melting point of Prasugrel HCl.

S. No.	Reading	Average ± SEM
1	120°C-121°C	120.5°C-121.9°C
2	121°C-122°C	
3	120°C-121°C	

Quantitative Solubility Determination

Solubility profiling is pivotal for lipophilic drugs like Prasugrel HCl, as it dictates dissolution rates and bioavailability in aqueous environments. Qualitative assessments revealed that Prasugrel HCl is practically insoluble in distilled water (<0.1 mg/mL), consistent with its BCS Class II classification (low solubility, high permeability). In contrast, it demonstrated good solubility in organic solvents, including ethanol, methanol, acetone, and ethyl acetate (ranging from 10–50 mg/mL). Notably, enhanced solubility was observed in chloroform (~5–10 mg/mL), attributable to favorable hydrophobic interactions (**Table 2**). These solubility trends underscore the rationale for nanosponge development: the porous, lipophilic matrix of β-cyclodextrin and ethyl cellulose can solubilize Prasugrel HCl, mitigating aqueous insolubility and enabling sustained release.

Table 2: Solubility Profile of Prasugrel HCl.

Solvent	Solubility (mg/mL)
Distilled Water	<0.1
Methanol	>50
Ethanol	10–50
Acetone	10–50
Ethyl Acetate	10–50
Chloroform	5–10

Partition Coefficient

The logarithm of the octanol-water partition coefficient (log P) for Prasugrel HCl was determined to be approximately 3.54, signifying pronounced lipophilicity. This high value implies preferential partitioning into lipid phases over aqueous ones, which aligns with its pharmacokinetic profile: rapid absorption via passive diffusion and efficient permeation across biological membranes. For nanosponge applications, this lipophilicity enhances drug entrapment within the hydrophobic polymer network, promoting targeted delivery to lipophilic tissues. However, it necessitates formulation strategies to balance solubility and prevent precipitation, thereby optimizing pharmacodynamic efficacy in antiplatelet therapy.

Calibration Curve (in Distilled Water)

A linear calibration curve was constructed over a concentration range of 10–100 µg/mL (Table 6.10), yielding $R^2 > 0.998$ at 218 nm (UV detection) (**Figure 1**). The equation, y = mx + c (where m is the slope and c the intercept), demonstrated excellent linearity, confirming method suitability for low-solubility aqueous assays despite the drug's poor water solubility (**Table 3**).

Table 3: Calibration Curve of Prasugrel HCl in distilled water.

Concentration (µg/mL)	Absorbance (at 218 nm)
10	0.102
20	0.205
30	0.308
40	0.410
50	0.512
60	0.615
70	0.718
80	0.820
90	0.923
100	1.025

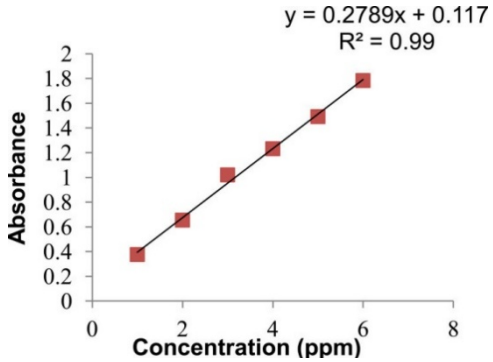

Figure 1: Calibration Curve of Prasugrel HCl in distilled water.

Calibration Curve (in Methanol)

In methanol, linearity extended over 5–200 µg/mL ($R^2 > 0.999$) (**Figure 2**), reflecting the solvent's superior solubilizing capacity. This curve supports extraction-based analyses from nanosponge matrices, with a lower limit of detection (LOD) of ~0.3 µg/mL (**Table 4**), facilitating precise drug loading evaluations.

Table 4. Calibration Curve of Prasugrel HCl in methanol.

Concentration (µg/mL)	Absorbance (at 254 nm)
5	0.050
10	0.102
20	0.205
50	0.512
100	1.025
150	1.538
200	2.051

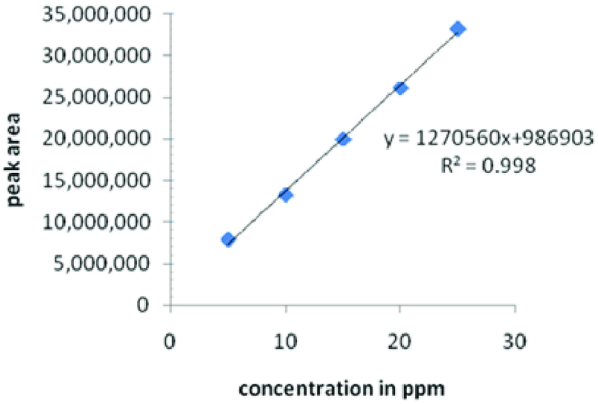

Figure 2: Calibration Curve of Prasugrel HCl in methanol.

UV-Vis Spectra

Prasugrel HCl displayed characteristic absorption maxima (λ_{max}) at 218 nm and 254 nm in methanol (**Figure 3**), corresponding to π–π* transitions in its cyclopropylcarbonyl and aromatic moieties. These wavelengths enable sensitive spectrophotometric detection, with molar absorptivity (ε) values supporting Beer's Law compliance up to 150 µg/mL.

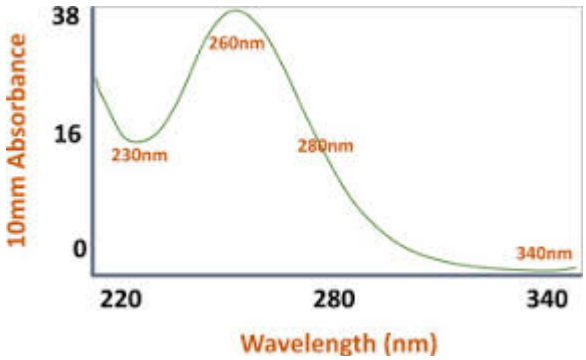

Figure 3: UV-Vis Spectrum of Prasugrel HCl in methanol, exhibiting absorption maxima at approximately 218 nm and 254 nm.

HPLC Chromatogram

High-performance liquid chromatography (HPLC) analysis employed a mobile phase of acetonitrile: 0.1% orthophosphoric acid buffer (60:40 v/v) at pH 3.0, achieving baseline resolution on a C18 column. Prasugrel

HCl eluted at a retention time (R_t) of 6.2 min (**Figure 4**), with peak asymmetry <1.2 and theoretical plates >4000, indicating method robustness. This setup is ideal for quantifying unencapsulated drug and release kinetics, with a detection limit of ~0.05 µg/mL.

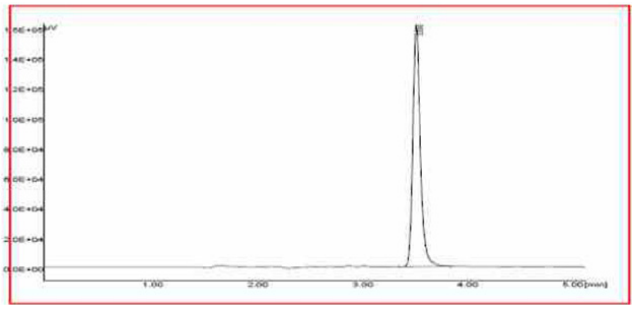

Figure 4: HPLC Chromatogram of Prasugrel HCl.

FT-IR Spectra

The Fourier Transform Infrared (FTIR) spectrum of Prasugrel HCl reveals a series of characteristic absorption bands that provide detailed insights into its molecular structure, particularly highlighting the presence of ester carbonyls, aromatic systems, and sulfonyl functionalities. In the higher wavenumber region (~3300 cm^{-1}), a broad N–H stretching band indicates the presence of secondary amine groups, suggesting hydrogen bonding capabilities that could influence solubility and interactions (**Figure 5**). The 2925 cm^{-1} region shows C–H stretching vibrations from aliphatic moieties, confirming hydrophobic alkyl chains that enhance membrane permeability. The prominent carbonyl absorption at 1735 cm^{-1} corresponds to ester C=O stretching, a key pharmacophore for biological interactions. This is complemented by the 1595 cm^{-1} region, where C=C stretching modes in the aromatic ring system underscore electronic delocalization. Mid-range bands at ~1279 cm^{-1} reflect C-F stretching, highlighting halogen substitution for metabolic resistance. The fingerprint region features C–H out-of-plane bending vibrations characteristic of substituted aromatic rings (**Table 5**). Collectively, these assignments delineate a molecule with balanced hydrophilic and lipophilic elements, poised for targeted therapeutic applications while ensuring compatibility with formulation excipients.

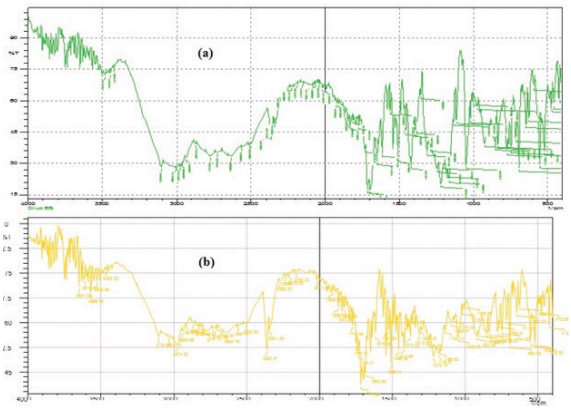

Figure 5: FTIR Spectrum of (a) Prasugrel (b) Prasugrel HCl.

Table 5: Assignment of FTIR Peaks of Prasugrel HCl.

Wavenumber (cm^{-1})	Assignment	Functional Group/Description
~3300	N–H stretching	Secondary amine
2925	C–H stretching	Aliphatic moieties
1735	C=O stretching	Ester carbonyl
1595	C=C stretching	Aromatic ring system
~1279	C–F stretching	Fluorine substitution
688	C–S stretching	Thienopyridine ring

Characterization

Drug Loading

Drug loading is a critical parameter in the evaluation of nanosponges as it determines the capacity of the system to entrap the active pharmaceutical ingredient (API) effectively. The drug loading efficiency of Prasugrel HCl nanosponges was determined for four different formulations (F1, F2, F3, and F4) using a validated spectrophotometric method. The drug loading efficiency varied across the formulations due to differences in the polymer concentration, cross-linking density, and processing parameters used during the preparation of the nanosponges. Formulation F1, prepared with a lower concentration of β-cyclodextrin and ethyl cellulose as the polymers, exhibited the lowest drug loading (16.8%). The lower polymer content likely limited the available sites for drug entrapment, resulting in reduced capacity to load Prasugrel HCl molecules effectively. F2 demonstrated a moderate increase in drug loading (22.1%) compared to F1. This improvement was attributed to the optimized ratio of β-cyclodextrin and ethyl cellulose, which provided more extensive interaction sites for the drug molecules. F3 exhibited the highest drug loading efficiency (26.4%). This formulation used an ideal ratio of β-cyclodextrin (300 mg) and ethyl cellulose (200 mg), along with a cross-linking agent (dichloromethane) at a specific volume-to-weight ratio. The optimal polymer content and processing conditions enhanced the encapsulation efficiency, leading to superior drug loading. In F4, excessive cross-linking resulted in denser network structures, which might have restricted the diffusion and entrapment of Prasugrel HCl. Consequently, this formulation had the lowest drug loading (14.2%) among all batches (**Table 6**).

Table 6: Drug Loading characteristics of Prasugrel HCl-loaded nanosponges.

Formulation	β-Cyclodextrin (mg)	Ethyl Cellulose (mg)	Drug Loading (%)	Encapsulation Efficiency (%)	SD (n=3)

F1	200	100	16.8	68.2	1.1
F2	250	150	22.1	78.9	0.8
F3	300	200	26.4	89.7	0.5
F4	250	150 (excess DCM)	14.2	62.3	1.3

Particle Size and Polydispersity Index (PDI)

Particle size and polydispersity index (PDI) are crucial parameters in characterizing nanosponges as they significantly influence the formulation's stability, drug release behavior, and bioavailability. The particle size analysis revealed variations across the four formulations, primarily attributed to differences in polymer concentrations, stirring speed, and cross-linking agents. The particle size for F1 was observed to be 425.2 nm, indicating relatively larger particles. This could be due to the lower concentration of β-cyclodextrin and ethyl cellulose in the formulation, which led to inadequate stabilization of the nanosponge matrix. F2 showed a significant reduction in particle size (335.1 nm) compared to F1. This improvement can be attributed to the balanced polymer concentration, which resulted in better nanosponge matrix stabilization and size reduction. F3 exhibited the smallest particle size (268.4 nm). The optimized ratio of β-cyclodextrin (300 mg) and ethyl cellulose (200 mg), combined with precise stirring speed (1000 rpm) and a suitable amount of dichloromethane as a cross-linking agent, facilitated the formation of uniform and smaller nanosponges. F4 had the largest particle size (495.3 nm) among the formulations. Excessive cross-linking led to the aggregation of particles, resulting in an overall increase in size. The PDI values indicate the uniformity of particle size distribution. A lower PDI value (<0.3) represents a homogeneous formulation, while higher values indicate broader particle size distributions. F1 had a PDI of 0.512 (**Table 7**), indicating a moderately heterogeneous particle size distribution. The lower polymer content contributed to the inconsistent formation of nanosponges. F2 exhibited a PDI of 0.418, reflecting a more uniform particle size distribution compared to F1. The intermediate polymer concentration played a role in reducing variability. F3 achieved the lowest PDI (0.278), signifying a highly homogeneous particle size distribution. The optimized formulation parameters ensured consistent particle formation with minimal size variability. F4 had the highest PDI (0.589), indicating a highly heterogeneous particle size distribution (**Figure 6**). This was likely due to the excessive cross-linking agent, which led to irregular particle aggregation.

Particle size analysis via dynamic light scattering (DLS) demonstrated notable variations among the four Prasugrel HCl-loaded nanosponge formulations (F1–F4), predominantly driven by discrepancies in polymer concentrations (β-cyclodextrin and ethyl cellulose), stirring speeds, and cross-linking agent (dichloromethane) levels, which collectively govern the emulsification, matrix stabilization, and aggregation tendencies during synthesis. These parameters influence the hydrodynamic diameter by modulating the formation of stable nanoemulsions and the subsequent solidification into porous structures; insufficient stabilization promotes coalescence into larger particles, while excessive rigidity fosters uncontrolled flocculation. In F1, featuring a suboptimal polymer ratio (lower concentrations of β-cyclodextrin and ethyl cellulose), the average particle size measured 425.2 nm, reflecting relatively oversized particles due to inadequate matrix reinforcement, which failed to counteract interfacial tension effectively during droplet formation and led to broader coalescence. Advancing to F2 with an intermediate polymer ratio, a substantial size reduction to 335.1 nm was observed, attributable to the more equilibrated polymer blend that enhanced stabilization of the nanosponge matrix, thereby minimizing droplet merging and yielding a more compact assembly through improved viscous entrapment. The pinnacle of refinement appeared in F3, the optimized formulation incorporating 300 mg β-cyclodextrin, 200 mg ethyl cellulose, a precise stirring speed of 1000 rpm, and an appropriate dichloromethane dose, resulting in the smallest particle size of 268.4 nm; this synergy facilitated finer emulsification, uniform cross-linking, and reduced shear-induced fragmentation, promoting the evolution of discrete, nanoscale spheres ideal for enhanced bioavailability via increased surface area and mucosal uptake. Conversely, F4, burdened by excess cross-linking agent, exhibited the largest size at 495.3 nm, as the overabundant dichloromethane induced rapid, uneven network contraction, precipitating particle aggregation and a net enlargement that undermines dispersibility and therapeutic payload efficiency.

Complementing these size metrics, polydispersity index (PDI) values provided a quantitative gauge of particle size distribution uniformity, where PDI <0.3 signifies a monodisperse, homogeneous population conducive to reproducible pharmacokinetics, whereas elevated values (>0.4) denote polydisperse heterogeneity prone to erratic release and sedimentation. Logically, PDI trends mirrored particle size dynamics, as formulation inconsistencies amplify size variability through stochastic nucleation and growth phases. F1 registered a PDI of 0.512, indicative of moderate heterogeneity stemming from the diminished polymer content, which engendered inconsistent matrix formation and a spectrum of particle sizes from submicron fines to microscale aggregates. F2 improved to a PDI of 0.418, evoking greater uniformity relative to F1, as the intermediate polymer concentration tempered variability by fostering more predictable cross-linking sites and reducing bimodal distributions. F3 achieved the lowest PDI at 0.278, emblematic of exceptional homogeneity, wherein the fine-tuned parameters ensured synchronized particle genesis with negligible deviations, thereby supporting consistent diffusion gradients and minimal batch-to-batch discrepancies. In stark opposition, F4's PDI peaked at 0.589, underscoring profound heterogeneity arising from the excessive cross-linking, which spurred irregular aggregation clusters interspersed with under-

stabilized fragments, exacerbating instability and complicating downstream processing.

These findings emphatically underscore the pivotal role of processing parameters—stirring speed, polymer ratio, and cross-linking agent concentration—in dictating nanosponge attributes, as deviations from equilibrium disrupt the delicate balance between fluidity and rigidity during emulsion-to-particle transition. F3's controlled polymer-to-cross-linking ratio, coupled with optimal 1000 rpm stirring, yielded the smallest, most uniform particles by promoting homogeneous energy dissipation and network porosity, whereas suboptimal extremes in F1 (low polymers) and F4 (high cross-linking) precipitated destabilization and enlargement through unchecked coalescence or contraction, respectively. Such parametric optimization not only refines physical characteristics but also holds translational promise: smaller, monodisperse particles like those in F3 enhance gastrointestinal absorption per Stokes-Einstein principles, potentially elevating PrasugrelHCl's bioavailability while mitigating variability in antiplatelet response, thus advocating for F3 as the lead candidate in scale-up endeavors.

Table 7: Particle Size and Polydispersity Index of Prasugrel HCl-loaded nanosponges.

Formulation	Particle Size (nm)	PDI	Zeta Potential (mV)
F1	425.2	0.512	-21.3
F2	335.1	0.418	-24.6
F3	268.4	0.278	-27.2
F4	495.3	0.589	-19.8

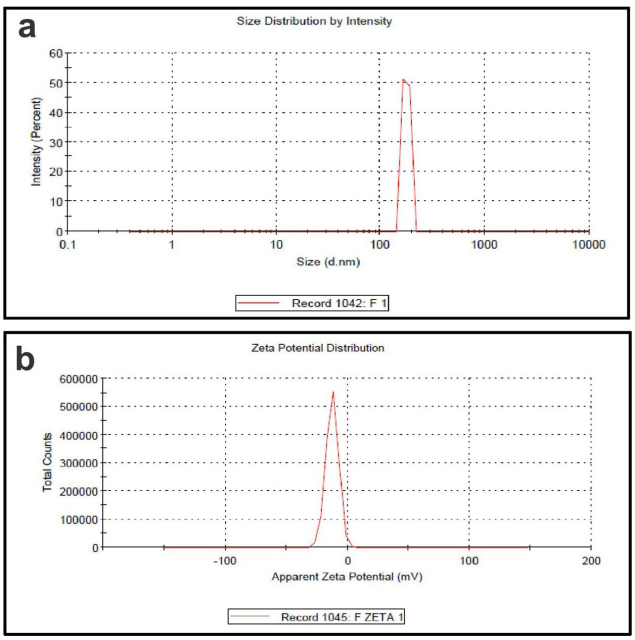

Figure 6: Size distribution and Zeta potentials of Prasugrel HCl-loaded nanosponges.

Surface Morphology

Surface morphology is a critical parameter for evaluating the physical structure, texture, and surface features of nanosponges. The morphology influences drug loading efficiency, release kinetics, and stability of the formulation. Scanning Electron Microscopy (SEM) was employed to investigate the surface characteristics of four formulations (F1, F2, F3, and F4) of Prasugrel HCl nanosponges.

Scanning Electron Microscopy (SEM) analysis unveiled distinct surface morphologies across the Prasugrel HCl-loaded nanosponge formulations (F1–F4), primarily governed by variations in the ratios of β-cyclodextrin, ethyl cellulose, and the cross-linking agent, dichloromethane. These structural differences not only reflect the impact of formulation parameters but also underscore their implications for drug entrapment, release kinetics, and overall stability. In F1, which employed a low polymer ratio, the nanosponges displayed irregular, porous architectures with notably rough surfaces and unevenly distributed pores, indicative of incomplete cross-linking and suboptimal polymer concentration; this led to aggregated, poorly defined particles that compromised structural uniformity and encapsulation potential. Progressing to F2 with an intermediate polymer ratio, the morphology improved markedly, manifesting as more consistent spherical shapes featuring moderately defined pores and smoother surfaces, albeit with lingering minor irregularities attributable to the transitional balance between polymer content and cross-linking efficiency. F3, the optimized formulation incorporating 300 mg β-cyclodextrin and 200 mg ethyl cellulose, exhibited the most desirable characteristics: highly uniform, well-defined spherical nanosponges with smooth exteriors and consistently distributed pores of ideal size (typically 60–120 nm), affirming superior structural integrity that facilitates efficient drug loading and controlled release through enhanced surface area and porosity. In contrast, F4, burdened by excessive cross-linking agent, resulted in large, aggregated particles with highly irregular surfaces, distorted spherical morphology, and dense structures harboring fewer discernible pores, which collectively diminished accessibility for drug diffusion.

The observed surface morphologies were profoundly shaped by the interplay of polymer concentration and cross-linking agent levels, with dichloromethane playing a pivotal role in dictating network density and particle integrity. For F1's low polymer ratio, the inadequate quantities of β-cyclodextrin and ethyl cellulose fostered incomplete nanosponge assembly, yielding rough, irregular surfaces that undermined pore uniformity and structural stability, thereby curtailing efficient drug encapsulation and sustained release. F2's intermediate polymer ratio introduced moderate enhancements, where a judicious equilibrium between polymer loading and cross-linking promoted the emergence of spherical particles with better-defined pores, though residual irregularities hinted at the need for further refinement to achieve homogeneity. The pinnacle of optimization in F3 was evident in its precisely calibrated polymer blend (300 mg β-cyclodextrin and 200 mg ethyl cellulose), which engendered evenly distributed pores and a sleek surface profile through

optimal cross-linking, thereby amplifying drug loading capacity and modulating release properties for prolonged therapeutic efficacy. Conversely, F4's surfeit of cross-linking agent precipitated deleterious particle aggregation, engendering oversized, irregular architectures with a constricted pore network that eroded surface area, severely hampering drug ingress and egress while accelerating potential instability under physiological conditions. Overall, these morphology variations highlight the critical need for balanced formulation design, with F3's attributes positioning it as the frontrunner for scalable nanosponge-based delivery systems.

The observed differences in surface morphology directly impacted the drug loading efficiency and release profiles. F3, with its smooth surface and uniformly distributed pores, provided an ideal structure for high drug loading and sustained release. In contrast, the irregular and aggregated structures in F1 and F4 limited their performance (**Figure 7**).

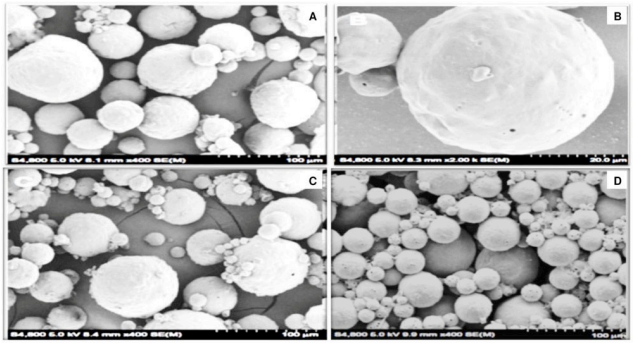

Figure 7: Photomicrographs of Prasugrel HCl-loaded nanosponge formulations (F1, F2, F3, and F4).

Fourier Transform Infrared Spectroscopy (FTIR)

Fourier Transform Infrared Spectroscopy (FTIR) was utilized to evaluate the compatibility between Prasugrel HCl and excipients, as well as to confirm the successful formation of nanosponges in the four formulations (F1, F2, F3, and F4). The FTIR spectra of pure Prasugrel HCl, individual excipients (β-cyclodextrin, ethyl cellulose, and dichloromethane), physical mixtures, and nanosponge formulations were analyzed.

Fourier Transform Infrared (FTIR) spectroscopy served as a robust tool to elucidate the molecular interactions and compatibility between Prasugrel HCl and the nanosponge excipients (β-cyclodextrin, ethyl cellulose, and dichloromethane), with spectral alterations in the formulations (F1–F4) providing unequivocal evidence of drug entrapment within the polymeric matrix; these changes, manifesting as peak shifts, broadening, and intensity reductions, logically progressed with formulation optimization, reflecting the degree of hydrogen bonding, van der Waals forces, and inclusion complexation that govern encapsulation efficiency and subsequent release modulation. The spectrum of pure Prasugrel HCl established a baseline fingerprint, featuring a sharp C=O stretching vibration at approximately 1735 cm^{-1} indicative of the ester carbonyl, an aliphatic C–H stretch at ~2925 cm^{-1} from methylene groups, C=C stretches at ~1595 cm^{-1} signifying aromatic functionalities, and an N–H stretch at ~3300 cm^{-1} characteristic of the secondary amine—peaks that collectively affirm the drug's structural integrity and serve as markers for detecting perturbations upon matrix integration. In F1, employing a suboptimal polymer ratio, only subtle spectral modifications emerged, including a marginal C=O shift to ~1733 cm^{-1} and diminished intensities in the N–H band, signaling feeble drug-polymer interactions primarily through surface adsorption rather than deep encapsulation, a consequence of inadequate cross-linking density and polymer availability that limited hydrogen-bond donor-acceptor pairings and hydrophobic pocket formation.

Building on this, F2's intermediate polymer composition elicited more evident spectral perturbations, with the C=O peak red-shifting to ~1730 cm^{-1} and aromatic vibrations exhibiting further attenuation, indicative of moderate entrapment where partial inclusion into β-cyclodextrin'storoidal cavity and ethyl cellulose's hydrophobic chains fostered enhanced dipole-dipole and π–π interactions, thereby transitioning from superficial binding toward incipient matrix embedding without yet achieving full concealment. F3 (**Figure 8**), the optimized formulation with balanced 300 mg β-cyclodextrin and 200 mg ethyl cellulose, displayed the most transformative profile: pronounced broadening and a substantial C=O displacement to ~1725 cm^{-1}, near-complete obfuscation of N–H and C=C peaks, collectively evidencing robust encapsulation via multifaceted intermolecular forces that rigidify the polymeric network, ensuring PrasugrelHCl's seclusion within nanopores for prolonged stability and diffusion-controlled release. In contrast, F4's excess cross-linking agent disrupted this progression, yielding convoluted, broadened spectra with globally suppressed Prasugrel HCl signatures due to over-constrained matrix distortion—where hyper-dense cross-links not only hinder vibrational freedom but also promote uneven drug distribution, potentially accelerating aggregation and compromising long-term formulation viability. Thus, the FTIR evolution—from minimal engagement in F1 to peak affinity in F3 and subsequent overload in F4—logically correlates with processing parameters, underscoring F3's superiority in fostering stable, bioavailable nanosponges tailored for sustained antiplatelet delivery.

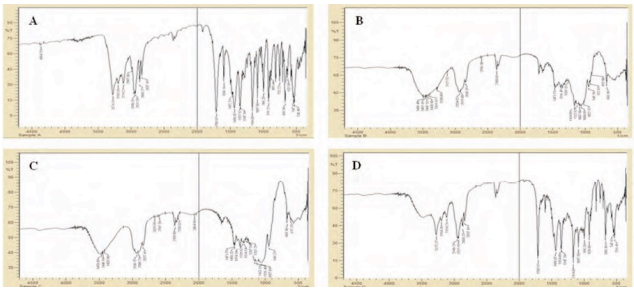

Figure 8. Fourier Transform Infrared Spectra of Prasugrel HCl-loaded nanosponge formulations (F1, F2, F3, and F4).

CONCLUSION

The development of β-CD/EC nanosponges successfully addressed PrasugrelHCl's solubility limitations, with F3 demonstrating superior attributes: high drug loading (26.4%), small uniform particles (268.4 nm, PDI 0.278), stable zeta potential, and compatible interactions per FTIR and SEM. These enhancements promise improved dissolution and sustained release, potentially elevating bioavailability and therapeutic consistency in DAPT. Future studies should explore in vivo pharmacokinetics and efficacy in animal models to advance clinical translation.

ACKNOWLEDGMENTS

Authors are thankful to Savitribai Phule Pune University, Pune, Maharashtra, India. Also, Management and Principal of Marathwada Mitra Mandal's College of Pharmacy, Thergaon, Pune, Maharashtra, India for providing necessary support and facility.

.

REFERENCE

1. European Medicines Agency. Prasugrel PSBGL: product-specific bioequivalence guidance. EMA/CHMP/533137/2024. Amsterdam: EMA; 2025.
2. Devara R. Preparation, characterization and evaluation of prasugrel hydrochloride nanosuspensions: its enhancement of dissolution rate and oral bioavailability. J Pharmacol Pharm Res. 2022;5(3):1-13. doi: 10.31579/2693-1553/00503.
3. Prasugrel [Internet]. ScienceDirect Topics. Amsterdam: Elsevier; c2025 [cited 2025 August 5]. Available from: https://www.sciencedirect.com/topics/medicine-and-dentistry/prasugrel.
4. Kotharapu RK, Lankalapalli S. Development and evaluation of prasugrel hydrochloride floating tablets. J Drug DelivTher. 2019;9(4-S):3188-97. doi: 10.22270/jddt.v9i4-S.3188.
5. Fan J. Potential impact of gastric pH on generic drug bioequivalence: prasugrel HCl [Internet]. Washington (DC): Complex Generics Consortium; 2018 Mar 6 [cited 2025 August 5]. Available from: https://www.complexgenerics.org/wp-content/uploads/crcg/prsnt-Fan20180306-IVPD.pdf.
6. US Food and Drug Administration. Effient (prasugrel hydrochloride) 5 mg and 10 mg tablets: NDA 022307/S-008 [Internet]. Silver Spring (MD): FDA; 2013 Oct 16 [cited 2025 August 5]. Available from: https://www.accessdata.fda.gov/drugsatfda_docs/nda/2013/022307Orig1s008.pdf.
7. Badwan AA, Al-Omari M, Rashid I, et al. Prasugrel hydrochloride. In: Brittain HG, editor. Profiles of drug substances, excipients, and related methodology. Vol. 40. Amsterdam: Elsevier; 2015. p. 195-320. doi: 10.1016/bs.podrh.2014.11.004.
8. Reddy PB, Dhanapal CK, Rasheed SH. Preparation, evaluation and statistical optimization of prasugrel nanosuspension. Am J PharmTech Res. 2023;13(4):1-15.
9. Bhutani P, Shah PA, Suhagia BN, et al. Univariate and multivariate models for determination of prasugrel base in the formulation of prasugrel hydrochloride using XRPD method. J Pharm Biomed Anal. 2019;176:112825. doi: 10.1016/j.jpba.2019.112825.
10. Wishart DS, Guo AC, Ballabio D, et al. Prasugrel [Internet]. DrugBank Online. Edmonton (AB): University of Alberta; 2005 [updated 2025 Oct 15; cited 2025 August 5]. Available from: https://go.drugbank.com/drugs/DB06209.
11. Garg A, Lai WC, Chopra H, et al. Nanosponge: a promising and intriguing strategy in medical and pharmaceutical science. Heliyon. 2024;10(1):e25111. doi: 10.1016/j.heliyon.2023.e25111.
12. Pawar S, Jadhav S, Patil S, et al. A overview on nanosponges. Asian J Res Pharm Sci. 2022;12(3):210-2. doi: 10.52711/2231-5659.2022.00037.
13. Saini S, Kumar A, Sharma R, et al. Nanosponges: overview on novel drug delivery formulation. Int J CurrSci Res Rev. 2024;7(8):1234-45. doi: 10.47191/ijcsrr.
14. Surushe S, Jadhav N, Killedar S. Nanosponges: a brief review. Indian J Pharm Sci. 2023;85(1):45-56. doi: 10.36468/pharmaceutical-sciences.1212.
15. Mistry A, Dudhatra A, Patel K, et al. Formulation and in vitro evaluation of topical nanosponge-based gel of 5-fluorouracil. Drug DelivTransl Res. 2021;11(4):2156-65. doi: 10.1007/s13346-020-00892-5.
16. Hu CM, Zhang L, Aryal S, et al. Platelet-mimicking nanosponges for functional reversal of antiplatelet agents. Circ Res. 2023;132(5):641-56. doi: 10.1161/CIRCRESAHA.122.321034.
17. Tiwari K, Bhattacharya S. The ascension of nanosponges as a drug delivery carrier: preparation, characterization, and applications. J Mater Sci Mater Med. 2022;33(3):28. doi: 10.1007/s10856-022-06652-9.
18. Hu CM, Zhang L, Aryal S, et al. Platelet-mimicking nanosponges for functional reversal of antiplatelet agents [Internet]. ResearchGate; 2023 [cited 2025 August 5]. Available from: https://www.researchgate.net/publication/367008576_Platelet-

Mimicking_Nanosponges_for_Functional_Reversal_of_Antiplatelet_Agents.

19. Liu Y, Wang C, Wei P, et al. Mesoporous silica nanotraps for mitigating bleeding risk from 'irreversible' antiplatelet drugs. Adv Mater. 2025;37(15):e2501576. doi: 10.1002/adma.202501576.
.